



Available online at: www.basra-science-journal.org



ISSN -1817 -2695

Synthesis, Characterization of Some Azo Dyes Derived From Sulfa Drugs and the Use of Them as Corrosion Inhibitors in 0.5M Hydrochloric Acid Solution

Adnan Sultan Abdul-Nabi* and Ekhlas Qanber Jasim**

* *Chemistry Department, College of Education for Pure Sciences, Basrah University, Basrah, Iraq*

** *Pharmaceutical Chemistry Department, College of Pharmacy, Basrah University, Basrah, Iraq*

Received 30-4-2013 , Accepted 28-7-2013

Abstract

Three azo dyes derived from sulfa drugs and pyridoxal were synthesized. The prepared compounds were identified by CHNS analysis FT-IR and ¹H-NMR spectroscopy. The prepared azo dyes were studied as corrosion inhibitors in 0.5M HCl solution by the weight loss and galvanostatic polarization techniques in the range of temperature 30, 40, 50 and 60°C. the results obtained revealed that A2 performed excellently as a corrosion inhibitor for C-steel in hydrochloric acid media and its efficiency attains 80% at 5x10⁻³M, time of 5hr and at 30°C. The efficiency of inhibitors was decreased as the temperature increases. The effect of temperature on the rate of corrosion in the absence and presence of these compounds was also studied. The Langmuir adsorption isotherm was tested for their fit to the experimental data. The apparent activation energies, Arrhenius constant, enthalpies and entropies of the dissolution process and the free energies and adsorption equilibrium constant for the adsorption process were determined and discussed. The fundamental thermodynamic functions were used to glean important information about A1, A2 and A3 inhibitory behavior.

Keywords: Azo dyes, corrosion, Tafel, thermodynamic properties.

1. Introduction

Corrosion is a fundamental process playing an important role in economics and safety, particularly for metals and alloys. Steel has found wide applications in a broad spectrum of industries and machinery; despite its tendency to corrosion. Corrosion inhibition of steel, therefore is a matter of theoretical as well as practical importance [1–8]. Acid solutions are widely used in industry, some of the important fields of applications being acid pickling of iron and steel, chemical cleaning and processing, or production and oil well acidification. The damage by corrosion generates not only high cost for inspection, repairing and replacement, but also these constitute a public risk, thus there is a necessity of developing novel substances that behave like corrosion inhibitors especially in acid media[9].

A large number of organic compounds including heterocyclic compounds [10-14] were studied as corrosion inhibitors for mild steel [15–17]. Most of them are toxic in nature. This has led to the development of non-toxic corrosion inhibitors such as Tryptamine[18], L-ascorbic acid [19], Sulfamethoxazole [20], and Cefatrexyl [21], Tramadol [22], Cefotaxime [23], sulfa drugs [24], antibacterial drugs [25], antifungal drugs [26], rhodanine azosulpha drugs [27].

Organic inhibitors react by adsorption on a metallic surface. Water molecules at metallic surface are replaced by organic inhibitor molecules. In the case of chemisorption, the formation of a bond between the metal and organic inhibitor impedes the anodic and cathodic processes, thereby protecting the metal surface [28]. Because organic inhibitors act by adsorption on the metal surface, the efficiency of these compounds depends strongly on their ability to form complexes with the metal. Both π electrons and polar groups containing sulfur, oxygen and/or nitrogen are fundamental characteristics of this type of inhibitor. The polar functional groups are usually considered the chelation center for chemical adsorption.[29]

This work aimed to synthesize and evaluate the inhibitory properties of three mono azo dyes compounds on the corrosion of carbon steel in 0.5 M HCl using weight loss and galvanostatic polarization techniques. Moreover, the effect of temperature on the dissolution carbon steel, as well as, on the inhibition efficiency of the studied compounds was also investigated and some thermodynamic parameters were computed.

2. Experimental part

Melting points were determined by open capillary and are uncorrected. The CHNS analysis measurements for the synthesized compounds were performed by using EuroVector model EA3000A (Italy) and ¹H-NMR spectra performed by using Bruker model ultra shield 300MHz (Switzerland), at the analytical Laboratory of

AL-ALBAYET University, Jordan. DMSO-d₆ was used as a solvent and TMS as an internal standard. IR spectra were recorded using KBr disc on Shimadzu FT-IR model 8400 Spectrophotometer at Chemistry Department, College of Education of Pure Sciences, Basrah University.

2.1. Synthesis of azo dyes

General procedure for the preparation of the compounds

The azo dyes compounds, **A1**: (E)-4-((4-formyl-5-hydroxy-3(hydroxymethyl)-6-methylpyridin-2-yl)diazenyl)-N-(pyridine-2-yl)benzenesulfonamide, **A2**: (E)-4-((4-formyl-5-hydroxy-3(hydroxymethyl)-6-methylpyridin-2-yl)diazenyl)-N-(5-methylisoxazol-3-yl)benzenesulfonamide and **A3**: (E)-N-(4,6-dimethylpyrimidin-2-yl)-4-((4-formyl-5-hydroxy-3-(hydroxymethyl)-6-methylpyridin-2-yl)diazenyl)benzenesulfonamide were prepared using the same method[30]

A mixture of sulfapyridine (0.92 g, 10 mmol), water (10 mL) and concentrated hydrochloric acid (2.62 mL, 30 mmol) was stirred until a clear solution was obtained. The mixture was cooled to 0–5 °C and a solution of sodium nitrite (0.76 g, 11 mmol) in water (5 mL) was then added dropwise,

maintaining the temperature below 5 °C. The resulting mixture was stirred for an additional 1h. Pyridoxal (2.4 g, 10 mmol) was dissolved in 8 mL aqueous NaOH (10 mmol) solution cooled to 0–5 °C in an ice bath. This solution was then gradually added to the solution of the cooled diazonium chloride and the resulting mixture was continually stirred at 0–5 °C for 2h. The mixture was left overnight. The resulting crude precipitate was filtered by acidification and washed several times with cold water, dried under vacuum, and then recrystallized from ethanol. The other azo compounds of A2 and A3 were synthesized in the same manner using sulfamethoxazole and sulfamethazine, as shown in Scheme 1. The physical properties of the prepared azo dyes were listed in Table 1.

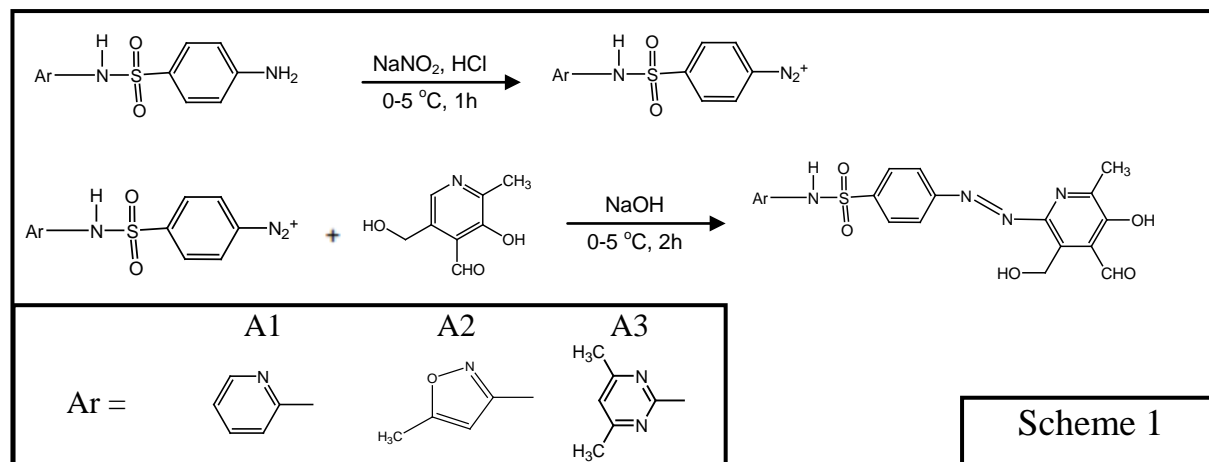


Table 1: The physical properties of the prepared azo dyes

Compd.	Molecular formula	Molecular weight (g/mole)	powder color and shape	m.p. (°C)	Yield (%)	Elemental analysis Found (Calcd.)			
						C%	H%	N%	S%
A1	C ₁₉ H ₁₇ N ₅ O ₅ S	427.43	Red powder	278	82	53.57 (53.39)	4.73 (4.01)	16.16 (16.38)	7.62 (7.5)
A2	C ₁₈ H ₁₇ N ₅ O ₆ S	431.42	Orange powder	230	78	50.44 (50.11)	3.99 (3.97)	16.29 (16.23)	7.26 (7.43)
A3	C ₂₀ H ₂₀ N ₆ O ₅ S	456.48	Brown powder	280	88	52.66 (52.62)	4.68 (4.42)	18.11 (18.41)	6.80 (7.02)

2.2. Solution preparation

The aggressive solutions, 0.5M HCl, were prepared by the dilution of AR grade 37% HCl in distilled water. The different concentrations of azo dye

compound were prepared by dissolving a certain amount of each compound in 0.5M HCl to obtain the following conc. (1×10^{-4} , 5×10^{-4} , 1×10^{-3} and 5×10^{-3} M).

2.3. Weight loss measurements[31]

Experiments were performed on a cold rolled steel (N80) of the following composition (wt.%): 0.85% Mn, 0.07% Ni, 0.05% P, 0.3% C, 0.21% Cu, 0.041S and the remainder Fe. All solutions were freshly prepared from analytical grade chemical

reagents. The mild steel strips of 3.5 cm 2.5 cm 0.4cm sizes were abraded with a series of emery paper (grade 120, 400, 600) and then washed with distilled water and acetone. After weighing accurately, the specimens were immersed in 50ml of 0.5M HCl with and

without addition of different concentrations of azo dyes inhibitor after different time (1-5)h, the strips were taken out washed, dried and weighed accurately. Duplicate

experiments were performed in each and the mean value of the weight loss was reported. Inhibition efficiency E%, surface coverage (θ) and corrosion rate was determined by using the following equation:

$$E\% = \left[\frac{W_{corr} - W_{corr(inh)}}{W_{corr}} \right] \times 100 \quad (1)$$

$$\theta = \frac{W_{corr} - W_{corr(inh)}}{W_{corr}} \quad (2)$$

where $W_{corr(inh)}$ and W_{corr} are the weight loss values in the presence and in the absence of inhibitor, respectively.

$$R_{corr.} = \frac{\Delta W \times K}{A \times D \times T} \quad (3)$$

Where ΔW = weight losses of metal (gram), K = constant (5.34×10^5), A = sample area (cm^2), D = metal density (g/cm^3) and T = exposed time (hr).

2.4. Electrochemical measurements[32]

Polarization studies were carried out using Bank EIEIKTRONKIK INTELLGENT CONTROLS Model MLab 200-ChemistryDepartment- Education College of pure sciences – Basrah University. Tafel polarization obtained by changing the electrode potential automatically from (+250 mV to -250 mV) at open circuit potential

with a scan rate 0.5 mV S^{-1} to study the effect of inhibitor on mild steel corrosion. The linear Tafel segment of cathodic and anodic curves were extrapolated to corrosion potential to obtain the corrosion current densities (I_{corr}). The inhibition efficiency was evaluated from the calculated I_{corr} values using the relationship:

$$E\% = \left[\frac{I_{corr} - I_{corr(inh)}}{I_{corr}} \right] \times 100 \quad (4)$$

where I_{corr} and $I_{corr(inh)}$ are the corrosion current in the absence and in the presence of inhibitor, respectively.

3. Results and discussion

3.1. FT-IR Spectra

FT-IR Spectra of the synthesized compounds were carried out using KBr disc method. The Spectra were shown in Figures

1-3 and the characterized bands were given in Table 2

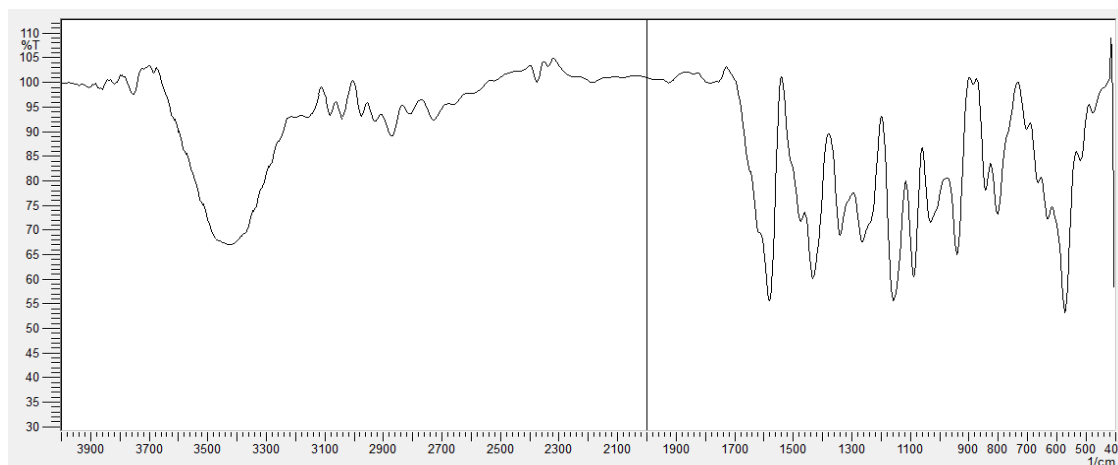


Figure 1: FT-IR Spectrum of A1 compound

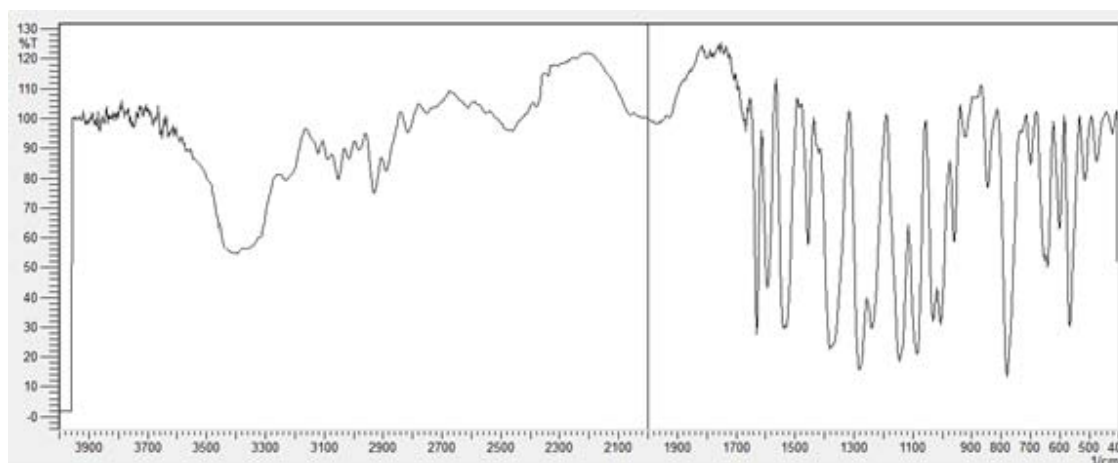


Figure 2: FT-IR Spectrum of A2 compound

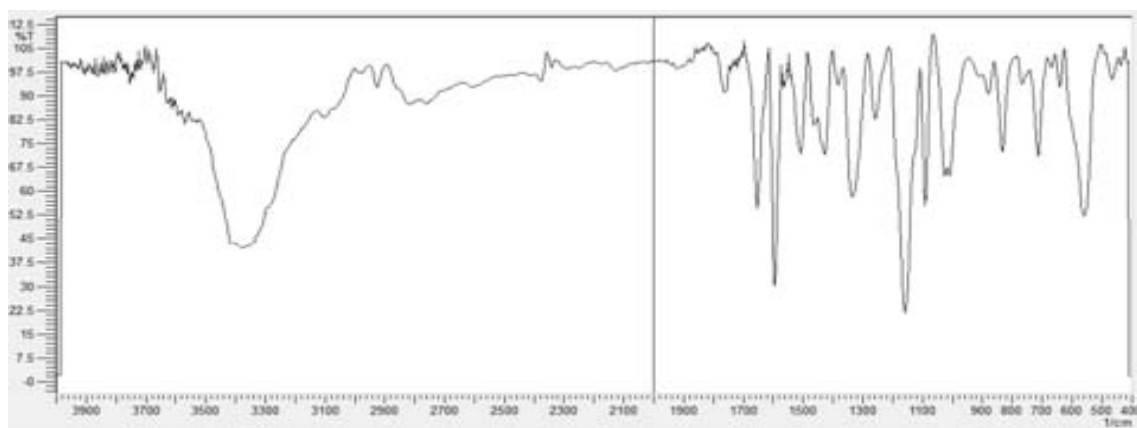


Figure 3: FT-IR Spectrum of A3 compound

Table 2: Characterized Bands in FT-IR Spectra for Prepared Azo Dyes

Comp.	ν O-H (cm^{-1})	ν C-H Arom. (cm^{-1})	ν C-H Aliph. (cm^{-1})	ν C=N (cm^{-1})	ν C=C (cm^{-1})	ν N=N (cm^{-1})	ν C-N (cm^{-1})
A1	3400 br	3114 w	2912 w	1616 s	1581 m	1431 m	1263 w
A2	3373 br	3051 w	2929 w	1629 s	1595 m	1456 m	1280 m
A3	3380 br	3097 w	2940 w	1652 s	1595 m	1427 w	1257 w

3.2. $^1\text{H-NMR}$

$^1\text{H-NMR}$ spectra of the prepared azo dyes were performed in deuterated dimethyl sulfoxide solutions with tetramethylsilane as an internal standard. All these spectra showed a peak at 2.5 ppm which was due to DMSO

solvent and some spectra showed a sharp peak at 3.33 ppm due to dissolved water in DMSO. Figures 4, 5 and 6 represent the $^1\text{H-NMR}$ spectra of the azo compounds and Table 3 represents the data of these Figures.

Table 3: $^1\text{H-NMR}$ data of the azo dyes compounds

Comp.	δ ppm (type of signal)							
	-CH ₃ Pyridoxal	-CH ₃ Sulfa	-CH ₂ - OH Pyridoxal	-CH ₂ - OH Pyridoxal	-CHO	-OH	-NH-	Aromatic system
A1	2.094(s)	-	3.791(s)	5.091(s)	9.204(s)	10.47(s)	10.67(s)	6.581- 7.827(m)
A2	2.343(s)	3.664(s)	4.599(s)	5.190(s)	9.190(s)	10.93(br)	11.64(br)	6.181- 8.044(m)
A3	2.342(s)	3.676(s)	4.275(s)	5.228(s)	9.223(s)	10.53(s)	10.87(br)	6.907- 8.292(m)

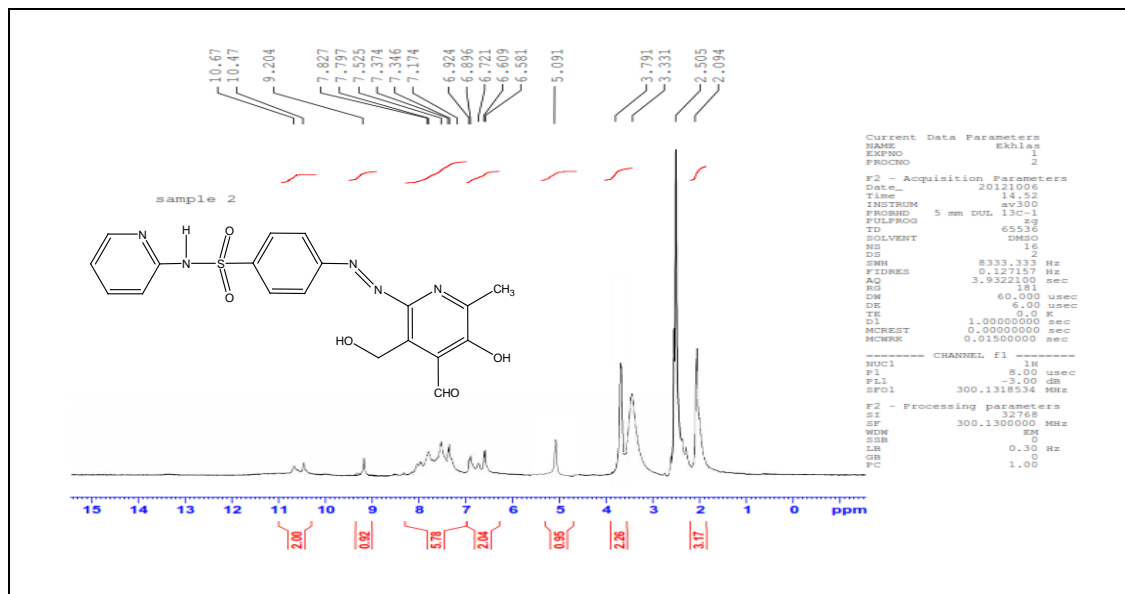


Figure 4: ¹H-NMR spectrum of the A1 compound

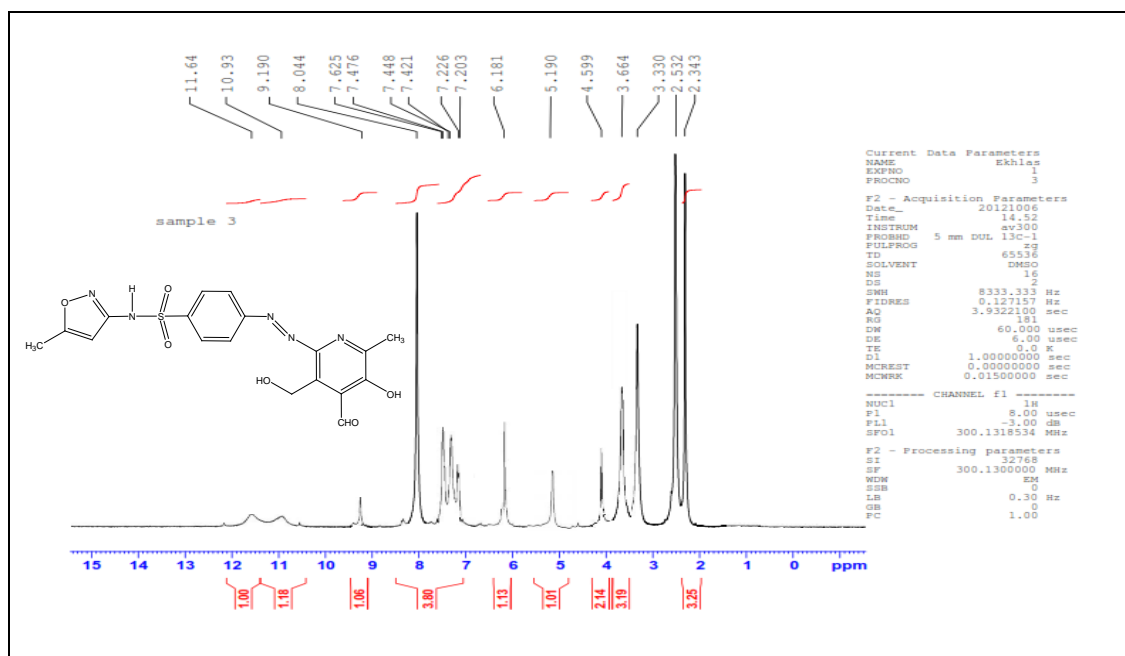


Figure 5: ¹H-NMR spectrum of the A2 compound

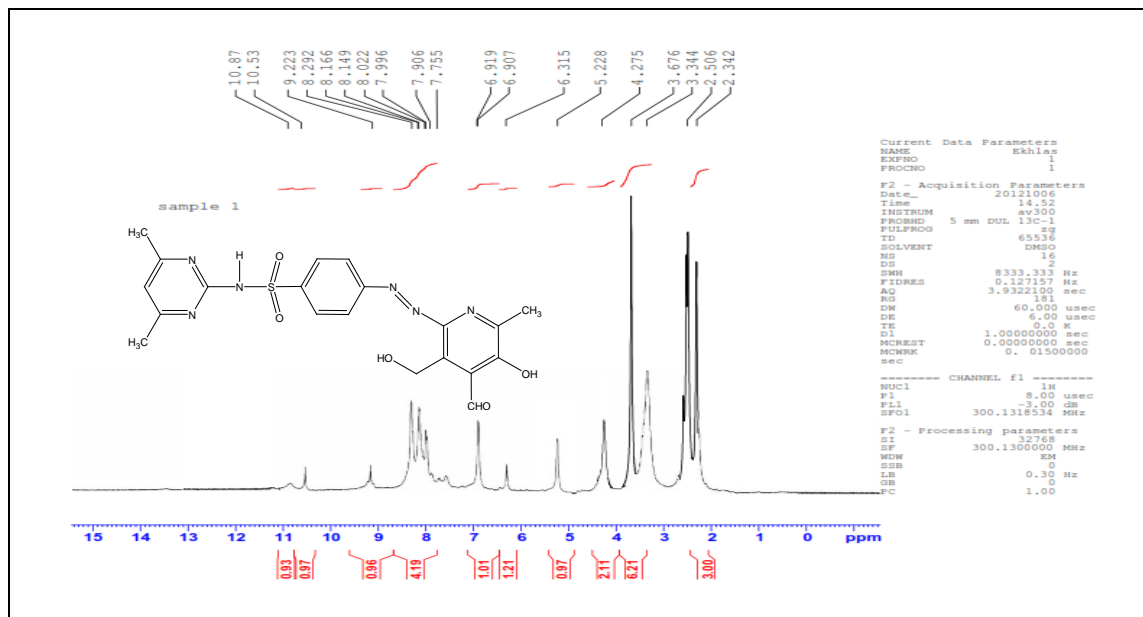


Figure 6: ¹H-NMR spectrum of the A3 compound

3.3. Weight loss measurements

3.3.1. Effect of immersing time:

The inhibition efficiency values of mild steel with the addition of azo dyes at fixed temperature are presented in Tables 4, 5 and 6. From these tables, it can be seen that inhibition efficiency values at fixed inhibitor concentration were increased as the

immersing time increased. This result is due to the fact that the adsorption amount and coverage of inhibitor on mild steel surface increases. Figures 7, 8 and 9 represent the variation of the inhibition efficiency IE% as function of the time.

3.3.2. Effect of temperature:

The values of inhibition efficiencies obtained from weight loss measurement for the different inhibitor concentrations in 0.5 M HCl are shown in Figures 10, 11 and 12. From these figures, it can be seen that the inhibition efficiency decreased with

increasing temperature, which indicates desorption of inhibitor molecule[33]. However, this decrease in *E*% is small at higher inhibitor concentration, as shown in Tables 7, 8 and 9.

3.3.3. Effect of inhibitor concentration:

The inhibition efficiency values at fixed time and temperature show that there is increasing in the efficiency by increasing the

concentration of inhibitor, and the best concentration is 5×10^{-3} M.

Table 4: Effect of azo dye compound A1 on the dissolution of C-steel in 0.5M HCl at different immersing time

Time (hr.)	1				2				3				4				5			
Conc. (M)	WL (gm)	Rcorr (mpy)	IE%	θ	WL (gm)	Rcorr (mpy)	IE%	θ	WL (gm)	Rcorr (mpy)	IE%	θ	WL (gm)	Rcorr (mpy)	IE%	θ	WL (gm)	Rcorr (mpy)	IE%	θ
blank	0.0039	92.80			0.0090	107.08			0.0165	130.88			0.0278	165.38			0.0356	169.42		
1×10^{-4}	0.0037	88.04	5.12	0.0512	0.0078	92.80	13.33	0.1333	0.0103	81.70	37.58	0.3758	0.0143	85.06	48.56	0.4856	0.0168	79.95	52.81	0.5281
5×10^{-4}	0.0036	85.66	7.69	0.0769	0.0063	74.96	30.00	0.3000	0.0091	72.18	44.85	0.4485	0.0121	71.98	56.47	0.5647	0.0147	69.95	58.71	0.5871
1×10^{-3}	0.0035	83.28	10.26	0.1026	0.0057	67.82	36.67	0.3667	0.0081	64.25	50.91	0.5091	0.0099	58.89	64.39	0.6439	0.0136	64.72	61.80	0.6180
5×10^{-3}	0.0032	76.15	17.95	0.1795	0.0051	60.68	43.33	0.4333	0.0073	57.90	55.76	0.5576	0.0094	55.92	66.19	0.6619	0.011	52.35	69.10	0.6910

Table 5: Effect of azo dye compound A2 on the dissolution of C-steel in 0.5M HCl at different immersing time

Time (hr.)	1				2				3				4				5			
Conc. (M)	WL (gm)	Rcorr (mpy)	IE%	θ	WL (gm)	Rcorr (mpy)	IE%	θ	WL (gm)	Rcorr (mpy)	IE%	θ	WL (gm)	Rcorr (mpy)	IE%	θ	WL (gm)	Rcorr (mpy)	IE%	θ
blank	0.0039	92.80			0.0090	107.08			0.0165	130.88			0.0278	165.38			0.0356	169.42		
1×10^{-4}	0.0031	73.77	20.51	0.2051	0.0061	72.58	32.22	0.3222	0.008	63.46	51.52	0.5152	0.0112	66.63	59.71	0.5971	0.0113	53.77	68.26	0.6826
5×10^{-4}	0.0032	76.15	17.95	0.1795	0.0054	64.25	40.00	0.4000	0.0066	52.35	60.00	0.6000	0.0099	58.89	64.39	0.6439	0.0101	48.06	71.63	0.7163
1×10^{-3}	0.003	71.39	23.08	0.2308	0.0048	57.11	46.67	0.4667	0.0057	45.21	65.45	0.6545	0.0089	52.95	67.99	0.6799	0.0098	46.63	72.47	0.7247
5×10^{-3}	0.0025	59.49	35.90	0.3590	0.0042	49.97	53.33	0.5333	0.0054	42.83	67.27	0.6727	0.006	35.69	78.42	0.7842	0.0071	33.78	80.06	0.8006

Table 6: Effect of azo dye compound A3 on the dissolution of C-steel in 0.5M HCl at different immersing time

Time (hr.)	1				2				3				4				5			
Conc. (M)	WL (gm)	Rcorr (mpy)	IE%	θ	WL (gm)	Rcorr (mpy)	IE%	θ	WL (gm)	Rcorr (mpy)	IE%	θ	WL (gm)	Rcorr (mpy)	IE%	θ	WL (gm)	Rcorr (mpy)	IE%	θ
blank	0.0039	92.80			0.0090	107.08			0.0165	130.88			0.0278	165.38			0.0356	169.42		
1×10^{-4}	0.0032	76.14	17.94	0.1794	0.0071	84.47	21.11	0.2111	0.0098	77.73	40.61	0.4061	0.0119	70.79	57.19	0.5719	0.0151	71.86283	57.58	0.5758
5×10^{-4}	0.0029	69.01	25.64	0.2564	0.0055	65.44	38.89	0.3889	0.008	63.46	51.52	0.5152	0.0127	75.55	54.32	0.5432	0.0133	63.2964	62.64	0.6264
1×10^{-3}	0.0027	64.25	30.77	0.3077	0.0043	51.16	52.22	0.5222	0.0071	56.32	56.97	0.5697	0.0082	48.78	70.50	0.7050	0.0091	43.30806	74.44	0.7444
5×10^{-3}	0.0028	66.63	28.21	0.2821	0.0039	46.40	56.67	0.5667	0.0066	52.35	60.00	0.6000	0.0071	42.24	74.46	0.7446	0.0083	39.50076	76.69	0.7669

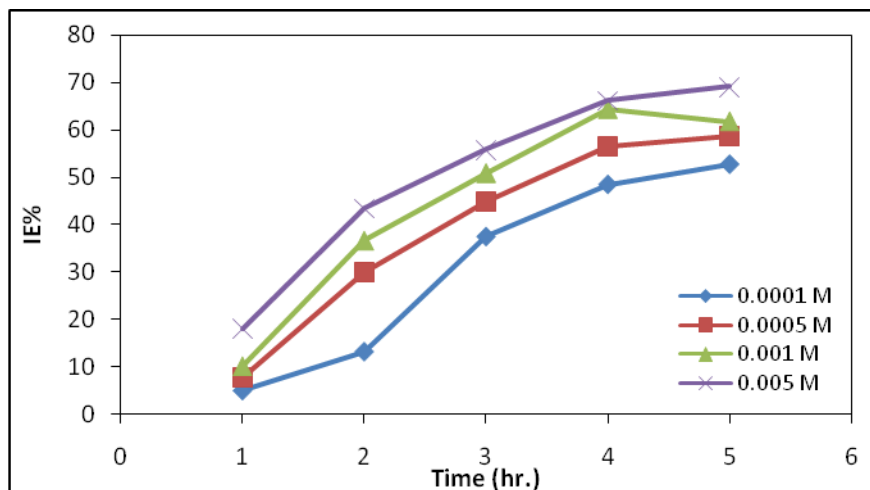


Figure 7: Inhibition Efficiency IE% as a Function of the Time in the Presence of Different Concentrations of A1 at 30°C

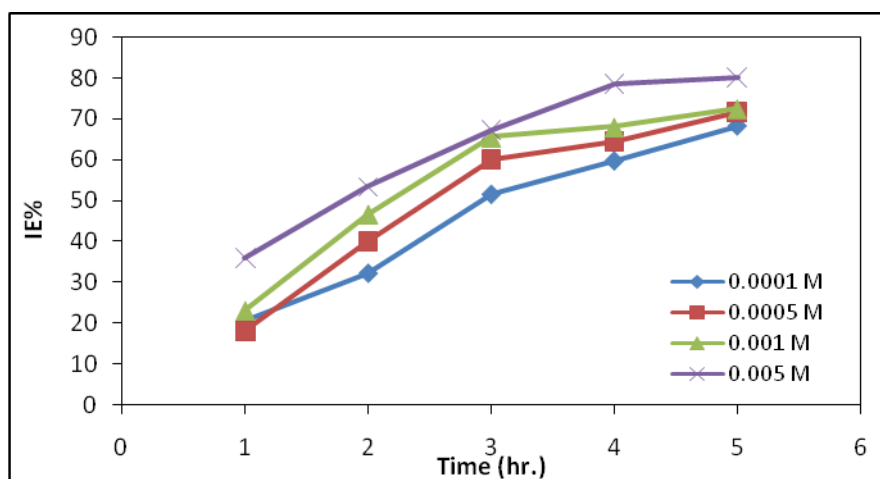


Figure 8: Inhibition Efficiency IE% as a Function of the Time in the Presence of Different Concentrations of A2 at 30°C

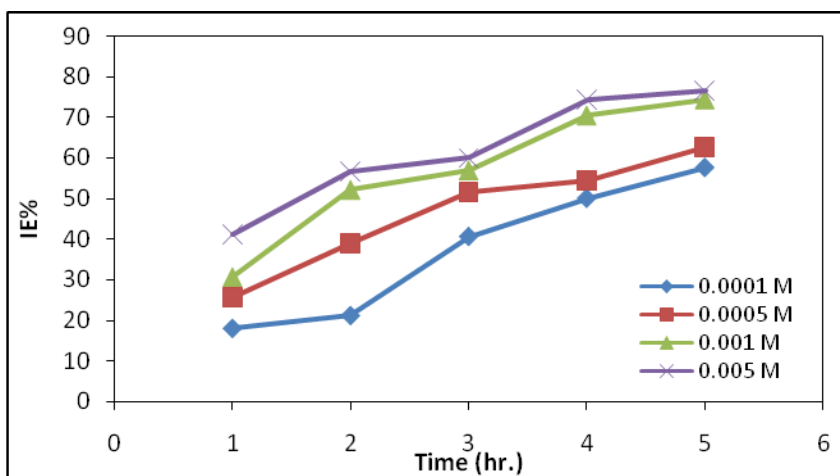


Figure 9: Inhibition Efficiency IE% as a Function of the Time in the Presence of Different Concentrations of A3 at 30°C

Table 7: Effect of azo dye compound A1 on the dissolution of C-steel in 0.5M HCl at different temperature

Temp. (°C)	30				40				50				60			
	Conc. (M)	WL (gm)	Rcorr (mpy)	IE%	θ	WL (gm)	Rcorr (mpy)	IE%	θ	WL (gm)	Rcorr (mpy)	IE%	θ	WL (gm)	Rcorr (mpy)	IE%
blank	0.0356	169.42			0.0592	281.74			0.0894	425.46			0.1211	576.33		
1x10 ⁻⁴	0.0168	79.95	52.81	0.5281	0.0321	152.7	45.78	0.4578	0.0544	258.89	39.15	0.3915	0.0797	379.30	34.19	0.3419
5x10 ⁻⁴	0.0147	69.95	58.71	0.5871	0.0274	130.40	53.72	0.5372	0.051	242.71	42.95	0.4295	0.0763	363.12	36.99	0.3699
1x10 ⁻³	0.0136	64.72	61.80	0.6180	0.02519	119.88	57.45	0.5745	0.0478	227.48	46.53	0.4653	0.0726	345.51	40.05	0.4005
5x10 ⁻³	0.011	52.35	69.10	0.6910	0.0203	96.61	65.71	0.6571	0.0408	194.17	54.36	0.5436	0.0634	301.72	47.65	0.4765

Table 8: Effect of azo dye compound A2 on the dissolution of C-steel in 0.5M HCl at different temperature

Temp. (°C)	30				40				50				60			
	Conc. (M)	WL (gm)	Rcorr (mpy)	IE%	θ	WL (gm)	Rcorr (mpy)	IE%	θ	WL (gm)	Rcorr (mpy)	IE%	θ	WL (gm)	Rcorr (mpy)	IE%
blank	0.0356	169.42			0.0592	281.74			0.0894	425.47			0.1211	576.33		
1x10 ⁻⁴	0.0113	53.78	68.26	0.6826	0.0242	115.17	59.12	0.5912	0.0439	208.93	50.89	0.5089	0.0678	322.67	44.01	0.4401
5x10 ⁻⁴	0.0101	48.07	71.63	0.7163	0.0221	105.18	62.67	0.6267	0.042	199.88	53.02	0.5302	0.0654	311.25	46.00	0.4600
1x10 ⁻³	0.0098	46.64	72.47	0.7247	0.02	95.18	66.22	0.6622	0.0388	184.65	56.60	0.5660	0.0603	286.98	50.21	0.5021
5x10 ⁻³	0.0071	33.79	80.06	0.8006	0.0153	72.81	74.16	0.7416	0.0311	148.01	65.21	0.6521	0.0481	228.91	60.28	0.6028

Table 9: Effect of azo dye compound A3 on the dissolution of C-steel in 0.5M HCl at different temperature

Temp. (°C)	30				40				50				60			
	Conc. (M)	WL (gm)	Rcorr (mpy)	IE%	θ	WL (gm)	Rcorr (mpy)	IE%	θ	WL (gm)	Rcorr (mpy)	IE%	θ	WL (gm)	Rcorr (mpy)	IE%
blank	0.0356	169.42			0.0592	281.74			0.0894	425.47			0.1211	576.33		
1x10 ⁻⁴	0.0151	71.86	57.58	0.5758	0.0277	131.83	53.21	0.5321	0.049	233.20	45.19	0.4519	0.077	366.45	36.42	0.3642
5x10 ⁻⁴	0.0133	63.30	62.64	0.6264	0.0244	116.12	58.78	0.5878	0.0422	200.84	52.80	0.5280	0.0749	356.46	38.15	0.3815
1x10 ⁻³	0.0091	43.31	74.44	0.7444	0.0188	89.47	68.24	0.6824	0.0347	165.14	61.19	0.6119	0.0666	316.96	45.00	0.4500
5x10 ⁻³	0.0083	39.50	76.69	0.7669	0.01577	75.05	73.36	0.7336	0.0281	133.73	68.57	0.6857	0.0601	286.02	50.37	0.5037

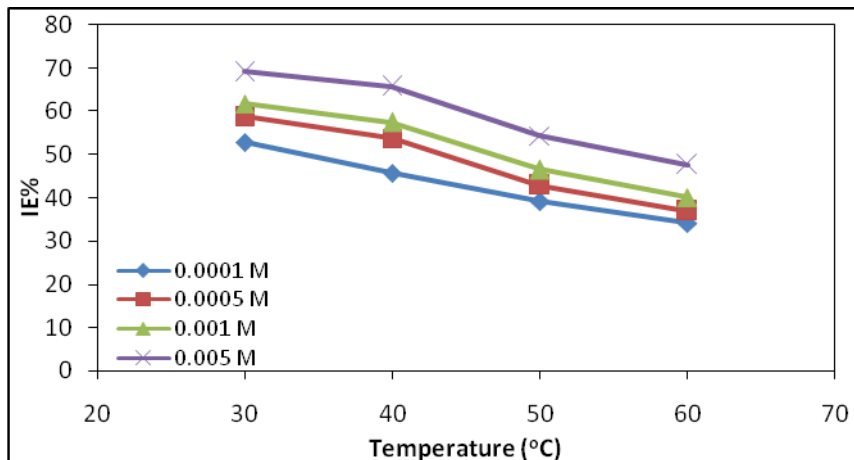


Figure 10: Inhibition Efficiency IE% as a Function of the Temperature in the Presence of Different Concentrations of A1 at 5 hrs

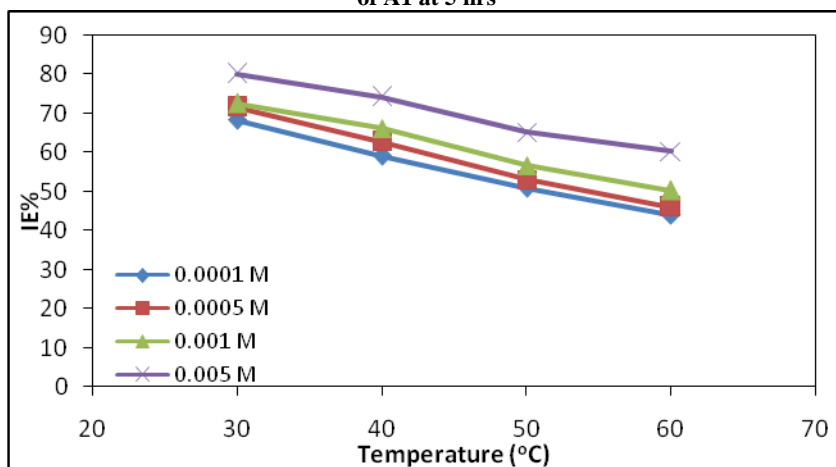


Figure 11: Inhibition Efficiency IE% as a Function of the Temperature in the Presence of Different Concentrations of A2 at 5 hrs

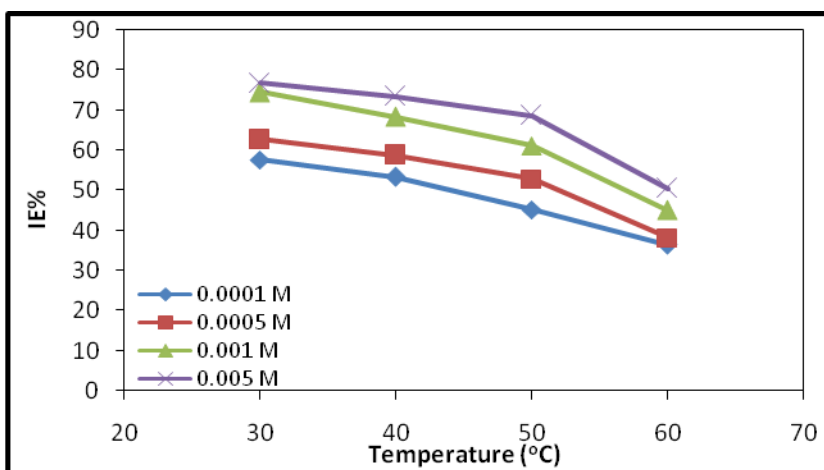


Figure 12: Inhibition Efficiency IE% as a Function of the Temperature in the Presence of Different Concentrations of A3 at 5 hrs

3.3.4. Adsorption isotherms

Basic information on the interaction between the inhibitor and the mild steel surface can be provided using the adsorption isotherm. For this purpose, the values of surface coverage (θ) at different concentrations of azo dyes in 0.5 M HCl acid in the temperature range (303–333 K) were calculated to explain the best isotherm to determine the adsorption process from the experimental data obtained.

Attempts were made to fit these θ values to various isotherm including Frumkin, Langmuir, Temkin, Freundlich isotherms. Byfar, the experimental data the results were best fitted by Langmuir adsorption isotherm equation [34]:

$$\frac{c}{\theta} = \frac{1}{K_{ads}} + C \quad (5)$$

Figures 13, 14 and 15 show the relationship between C/θ and C at temperature ranges studied. These results show that all the linear correlation coefficients (R^2) are almost equal to unity and all the slopes are very close to unity, which indicates that the adsorption of azo dyes follows Langmuir adsorption isotherm, which means that the solid surface contains a fixed number of adsorption sites and each site holds one adsorbed species.

The equilibrium constant of the adsorption process, K_{ads} , is related to the free energy of adsorption, ΔG°_{ads} , by:

$$K_{ads} = \frac{1}{55.5} \exp\left(\frac{-\Delta G^{\circ}_{ads}}{RT}\right) \quad (6)$$

From this relationship, ΔG_{ads} can be calculated as -33.94, -33.75 and -32.83 kJ mol⁻¹ for the inhibitors A2, A3 and A1, respectively. The large negative values of ΔG indicate the spontaneous adsorption of azo dyes on mild steel surface. Generally, values of ΔG_{ads} around -20 kJ mole⁻¹ or lower are consistent with physisorption and those around -40 kJ mole⁻¹ or higher involves chemisorption.

The large value of K at 303K indicates that A2 (12821 mole⁻¹) is strongly adsorbed on the mild steel surface as compared with A3 and A1 (11877 and 8250 mole⁻¹, respectively), and these value were decreased as the temperature increases, as shown in Table 10.

Table 10: Linear correlation coefficient R^2 , equilibrium constant K and the free energy of adsorption ΔG_{ads} of azo inhibitors

Temp (K)	A1			A2			A3		
	K (mol ⁻¹)	ΔG_{ads} , KJmol ⁻¹	R^2	K (mol ⁻¹)	ΔG_{ads} , KJmol ⁻¹	R^2	K (mol ⁻¹)	ΔG_{ads} , KJmol ⁻¹	R^2
303	8250	-32.8354	0.9999	12821	-33.946	0.9995	11877	-33.7533	0.9994
313	6227	-33.187	0.9999	8900	-34.1164	0.9980	8439	-33.978	0.9995
323	4580	-33.4223	0.9988	6292	-34.2752	0.9986	5962	-34.1305	0.9976
333	3642	-33.8226	0.9984	5475	-34.9512	0.9981	4444	-34.3736	0.9990

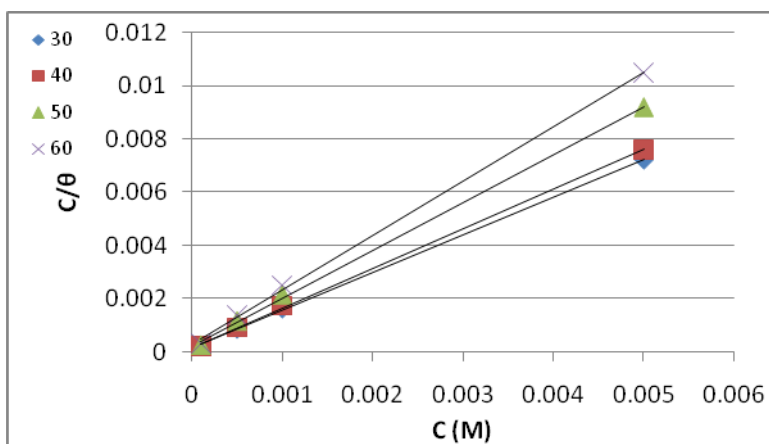


Figure 13: Langmuir adsorption isotherm of the used inhibitors A1 at different temperature

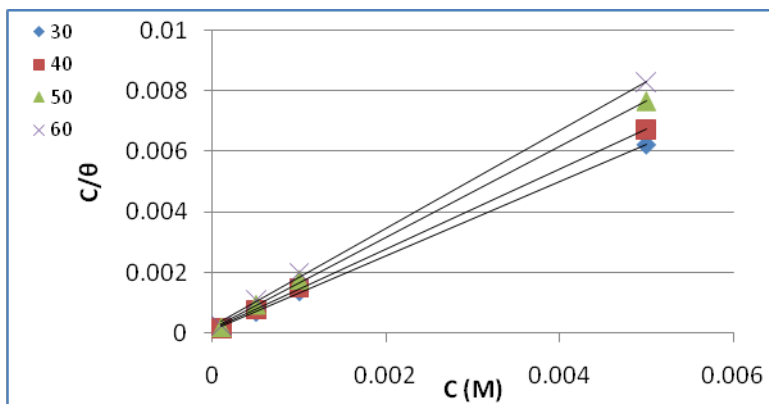


Figure 14: Langmuir adsorption isotherm of the used inhibitors A2 at different temperature

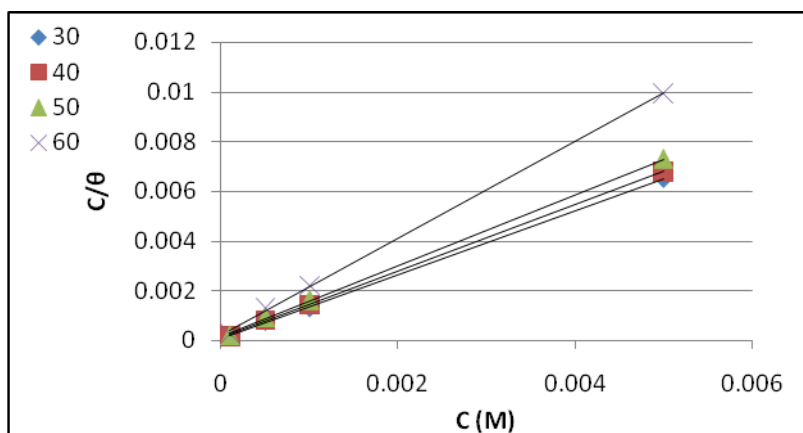


Figure 15: Langmuir adsorption isotherm of the used inhibitors A3 at different temperature

3.3.5. Thermodynamic parameters

Thermodynamic parameters are important to study the inhibitive mechanism. The thermodynamic functions for dissolution of mild steel in the absence and in the presence of various concentrations of azo dyes were obtained by applying the Arrhenius equation and the transition state equation:

$$\log(R_{corr}) = \frac{-E_{act}}{2.303 RT} + \log A \quad (7)$$

$$R_{corr} = \frac{RT}{Nh} \exp\left(\frac{\Delta S}{R}\right) \exp\left(-\frac{\Delta H}{RT}\right) \quad (8)$$

Where E_a apparent activation energy, A Arrhenius factor, the apparent enthalpy ΔH of activation, ΔS the apparent entropy of activation, h the Planck's constant and N the Avogadro number.

Table 11: Activation energy, Arrhenius factor, the enthalpy ΔH of activation and the entropy of activation of azo inhibitors

Conc.	A1				A2				A3			
	A	Ea	ΔH	$-\Delta S$	A	Ea	ΔH	$-\Delta S$	A	Ea	ΔH	$-\Delta S$
	$\times 10^8$	(KJmol-1)			$\times 10^8$	(KJmol-1)			$\times 10^8$	(KJmol-1)		
Blank	1.468	34.34	31.71	0.097	1.468	34.34	31.71	0.097	1.468	34.34	31.71	0.097
1x10-4	16.67	43.71	41.07	0.073	26.24	44.34	47.60	0.054	33.88	43.59	43.20	0.067
5x10-4	21.42	46.73	44.10	0.064	66.37	47.31	48.77	0.052	22.28	44.55	45.44	0.061
1x10-3	41.30	47.59	44.96	0.062	181.9	50.58	49.90	0.048	32.73	45.12	51.93	0.043
5x10-3	102.3	49.99	47.35	0.056	173.7	50.96	51.60	0.045	44.87	46.31	52.60	0.040

From Table 11, the higher values of E_a and ΔH in the presence of inhibitor rather than without inhibitor indicated that as the temperature is raised a decrease in protection efficiency is obtained. The negative value of ΔS implies that the activation complex represents an association rather than a disordering take place going from reactants to the activated complex.[35]

that dissolution of steel is difficult. Values of E obtained in the presence of inhibitor are higher than those for the uninhibited one, indicating a strong inhibitive action for the studied compounds by increasing the energy barrier for the corrosion process, emphasizing the electrostatic character of the inhibitor adsorption on mild steel surface.

The positive sign of the enthalpy is an endothermic nature of the steel dissolution in 0.5M HCl solution meaning

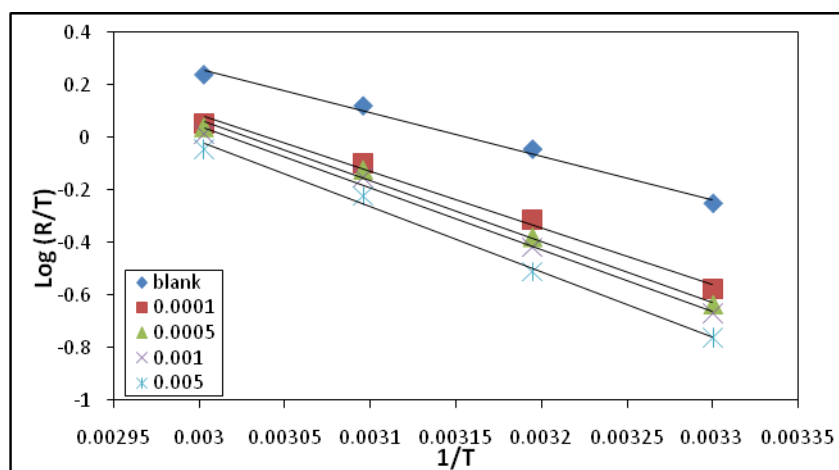


Figure 16 : Arrhenius plots $\text{Log}(R_{\text{corr.}}/T)$ versus $1/T$ at different concentration of A1

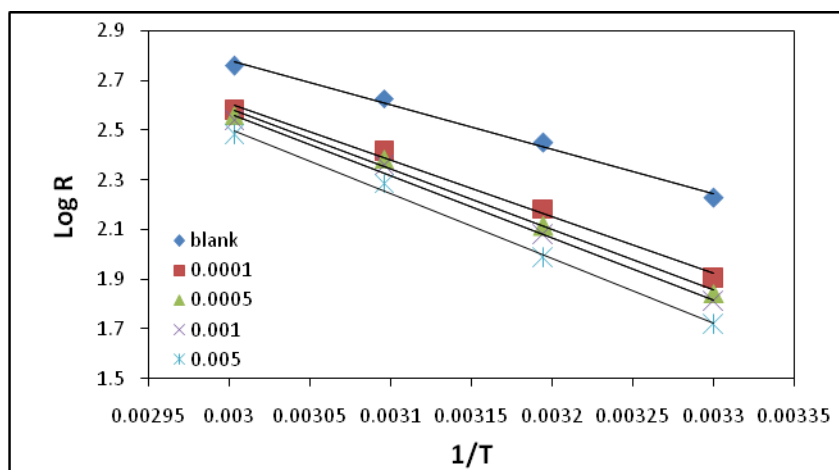


Figure 17 : Arrhenius plots $\text{Log } R_{\text{corr.}}$ versus $1/T$ at different concentration of A1

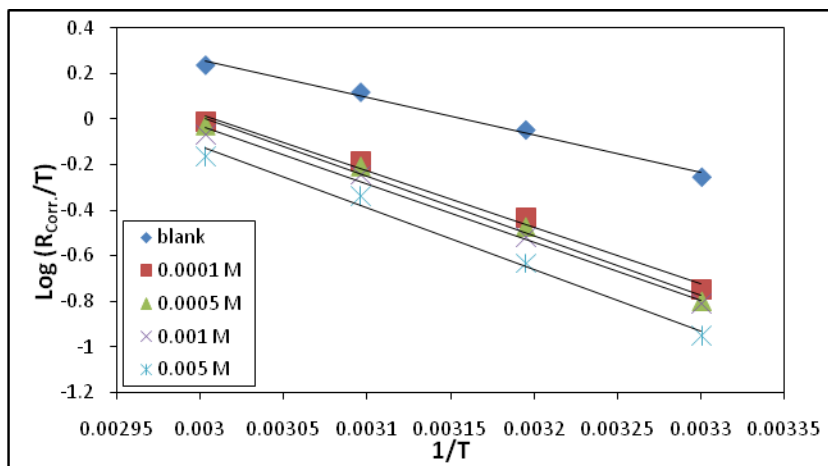


Figure 18 : Arrhenius plots $\text{Log}(R_{\text{corr.}}/T)$ versus $1/T$ at different concentration of A2

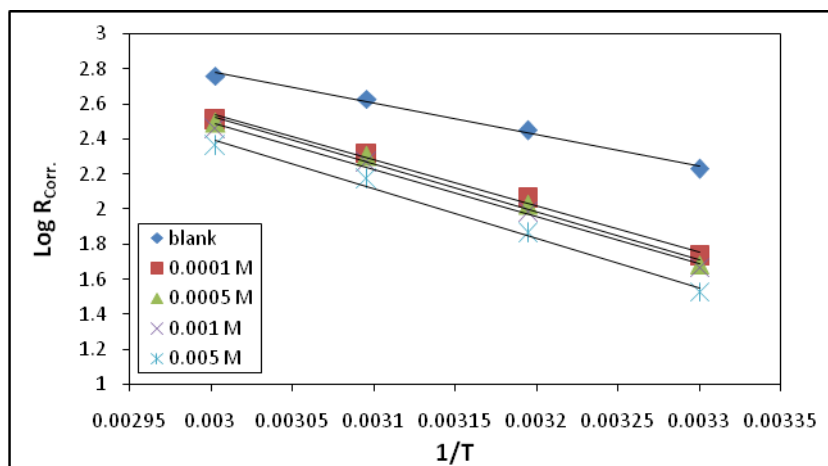


Figure 19 : Arrhenius plots $\text{Log } R_{\text{corr.}}$ versus $1/T$ at different concentration of A2

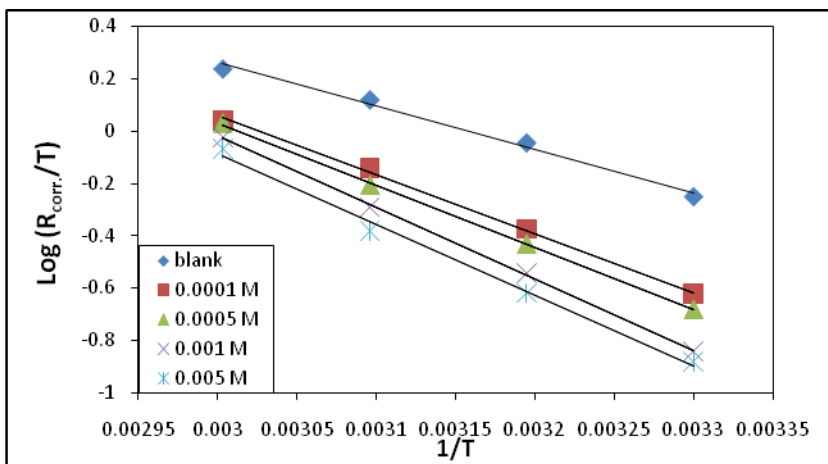


Figure 20 : Arrhenius plots $\text{Log}(R_{\text{corr.}}/T)$ versus $1/T$ at different concentration of A3

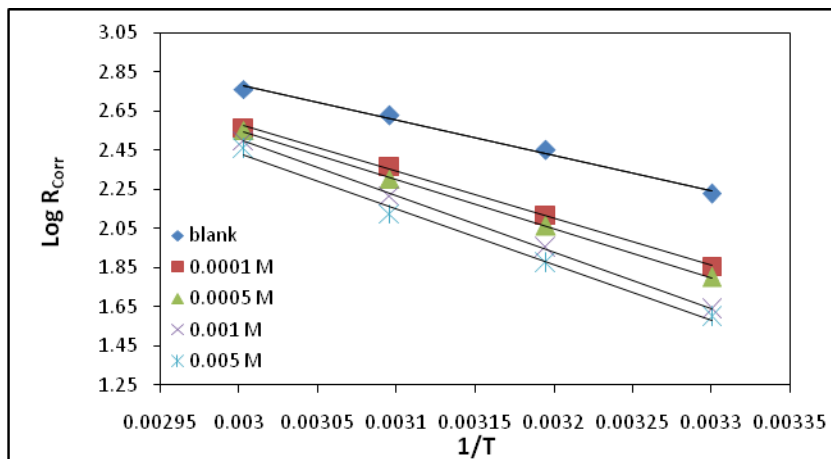


Figure 21: Arrhenius plots Log R_{corr} versus $1/T$ at different concentration of A3

3.4. Potentiodynamic polarization measurements

The electrochemical kinetics of metallic corrosion process can be characterized by determining at least three polarization parameters, such as corrosion current density (I_{corr}), corrosion potential (E_{corr}) and Tafel slopes (β_a and/or β_c). The corrosion behavior can be determined by a polarization curve (E versus $\log i$). The evaluation of the polarization parameters leads to the determination of the corrosion rate (C_R).

Thus, it was possible to determine I_{corr} for all concentrations of all tested inhibitors, as well as for the blank

(solution without inhibitor). The polarization curves for the carbon steel (C-steel) electrode in 0.5 M HCl with different inhibitors at $5 \times 10^{-3} M$ and at different temperatures are shown in Figure 16. The electrochemical parameters, namely, the corrosion potential (E_{corr}), corrosion current density (I_{corr}), anodic (β_a) and cathodic (β_c) Tafel slopes and inhibition efficiency (E), are listed in Table 10.

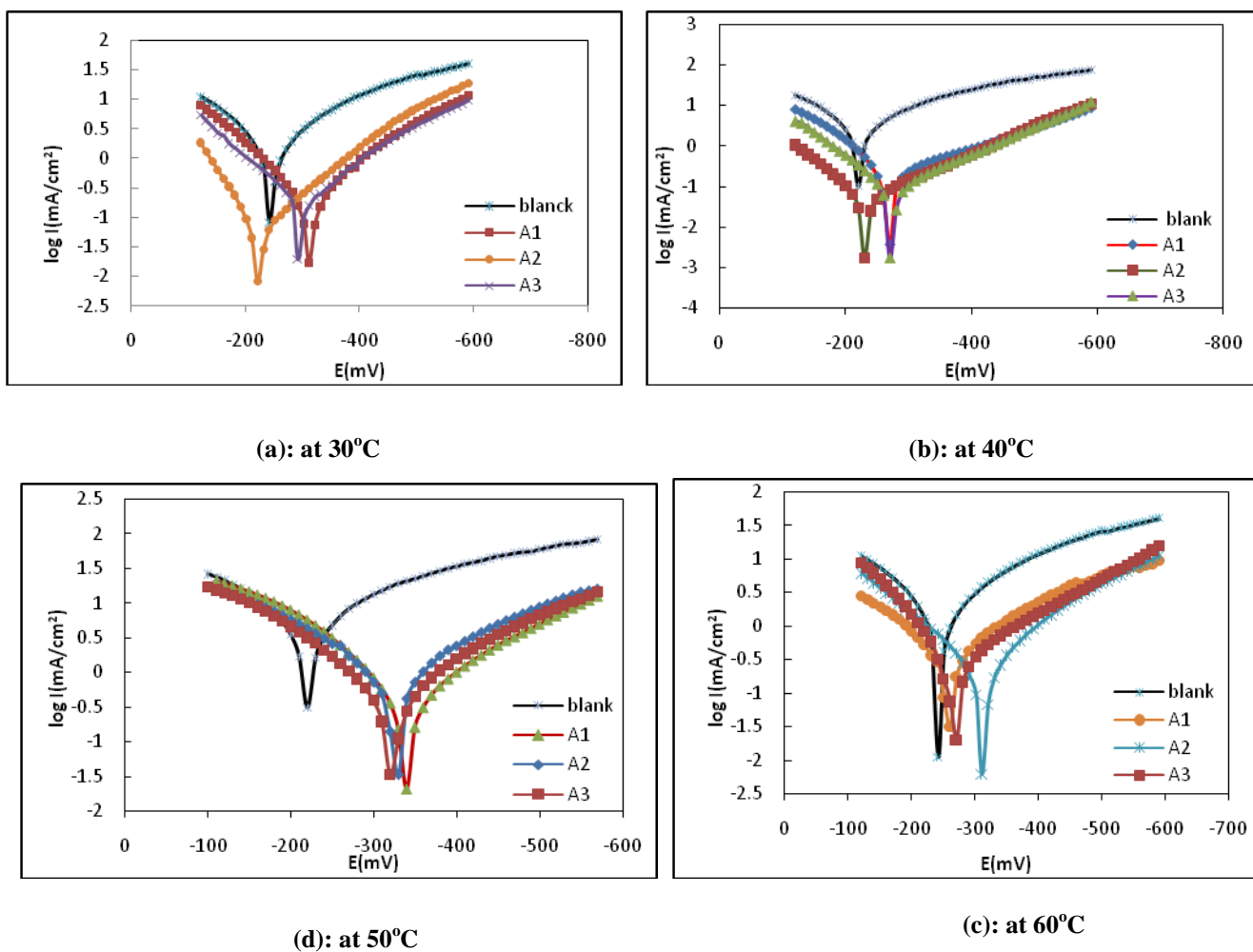


Figure 16: Anodic and cathodic polarization curves (Tafel curves) of mild steel in 0.5 M HCl and in the absence and presence of $5 \times 10^{-3}\text{M}$ of Inhibitor (A1, A2 and A3) at various temperatures

Table 10: Electrochemical parameters for corrosion of mild steel in 0.5M HCl in the presence of different inhibitors at various temperatures

Inhibitor Conc. (ppm)	I_{corr} μ A/cm ²	E_{corr} mV	β_c mV/dm	β_a mV/dm	E%
30 °C					
Blank	504.77	-241.2	-113.1	95.2	
A1	137.6	-311.1	-96.5	94.7	72.74006
A2	88	-230.7	-97.4	99.6	82.56632
A3	119.6	-271.5	-103.9	100.3	76.30604
40 °C					
Blank	755.8	-273.2	-99.2	110.7	
A1	250.6	-327.1	-95.9	82.6	66.84308
A2	170.4	-232.3	-97.8	93.9	77.45435
A3	198.6	-285.3	-112.7	108.4	73.72321
50 °C					
Blank	839.2	-279.8	-120	107.5	
A1	312.7	-340.2	-89.5	81.4	62.73832
A2	220.9	-349.7	-107.3	88.2	73.67731
A3	247.2	-338.4	-122.9	134.2	70.54337
60 °C					
Blank	891.8	-289.6	-107.3	103.2	
A1	364.2	-349.6	-79.8	71.6	59.16125
A2	311.7	-350.4	-123.9	78.6	65.04822
A3	351.3	-340.4	-126.7	142.8	60.60776

From Table 10, we found that by increasing the temperature, the current density increases, which led to decrease

the corrosion efficiency. This may be attributed to the decrease of the adsorption process of inhibitor on the metal surface.

3.5. Mechanism of inhibition

A clarification of mechanism of inhibition requires full knowledge of the interaction between the protective compound and the metal surface. Many of the organic corrosion inhibitors have at least one polar unit with atoms of nitrogen, sulfur, oxygen and in some cases phosphorous. It has been reported that the inhibition efficiency decreases in the order

to $O < N < S < P$. The polar unit is regarded as the reaction center for the chemisorptions process. Furthermore, the size, orientation, shape and electric charge on the molecule determine the degree of adsorption and hence the effectiveness of inhibitor. On the other hand, iron is well known for its coordination affinity to heteroatom bearing ligands. Increase in

inhibition efficiencies with the increase of concentration of azo dyes show that the inhibition action is due to the adsorption on the steel surface. Four types of adsorption may take place by organic molecules at metal/solution interface namely.

- (1) Electrostatic attraction between the charged molecules and charged metal.
- (2) Interaction of unshared electron pairs in the molecule with the metal.
- (3) Interaction of p-electrons with the metal.
- (4) Combination of (1) and (3) [36].

The results indicated that the %IEs of mono azo dye compounds is more or

less, dependent on the nature of constituents. The order of inhibition efficiency obtained from weight loss and polarization techniques decreases in the following order: $A2 > A3 > A1$, as shown in Figure 17. The mono azo dye derivatives used in the present investigation have an electron donating groups $-CH_3$ and $-OH$, and electron withdrawing group such $-CHO$. On the other hand, presence of unshared electron pairs in the molecule O, N and S, and all these groups gave good effect on the corrosion inhibitor, as shown in Figures 18-20.

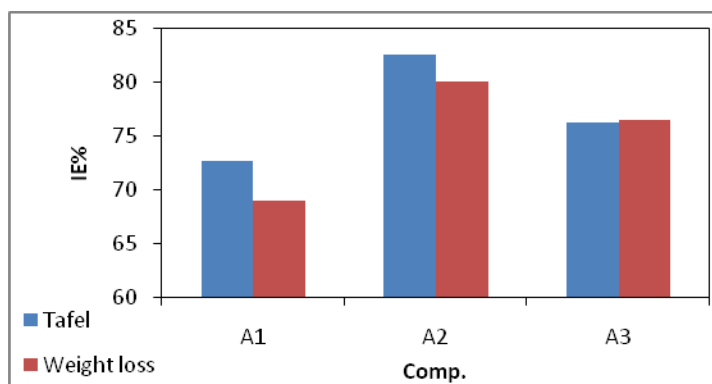


Figure 17: Inhibitor efficiency of the azo dyes by weight loss and Tafel methods

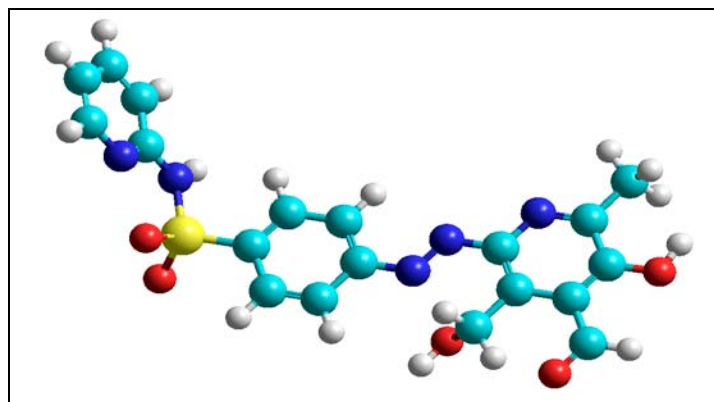


Figure 18: Three-dimensional representation of A1 molecule

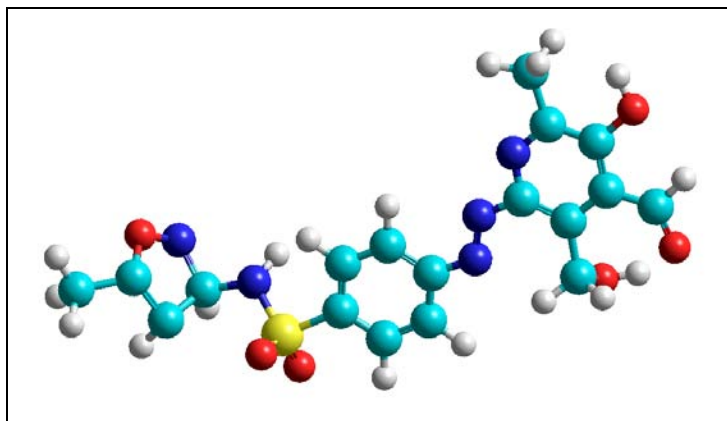


Figure 19: Three-dimensional representation of A2 molecule

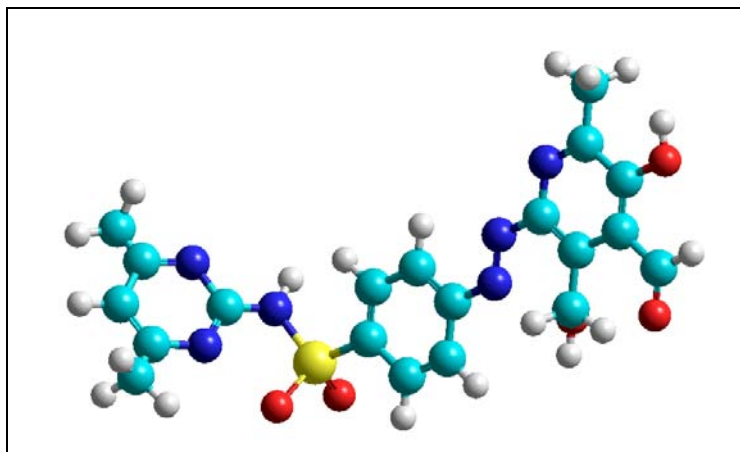


Figure 20: Three-dimensional representation of A3 molecule

4. Conclusion

(1) Azo dyes act as good inhibitors for the corrosion of mild steel in 0.5 M HCl.
(2) The inhibition efficiency of azo dyes decreased with temperature, which leads to an increase activation energy of corrosion process.
(3) The adsorption of azo dyes obey Langmuir adsorption isotherm. The

adsorption process is a spontaneous and high value of equilibrium constants.
(4) Potentiodynamic polarization curves reveal that azo dyes are mixed-type but predominantly cathodic inhibitors.
(5) The results obtained from weight loss and polarization studies are in a good agreement.

References:

- [1] Z. Wahbi, A. Guenbour, H. Abou El Makarim, A. Ben Bachir and S. El Hajjaji, *Porg. Org. Coat.*, **60**, 224(2007).
- [2] K.F. Khaled, *Electrochim. Acta* **53**, 3484(2008).
- [3] K.F. Khaled, *Appl. Surf. Sci.* **252**, 4120(2006).
- [4] M.A. Amin, S.S. Abd El Rehim and H.T.M. Abdel-Fatah, *Corros. Sci.*, **51**, 882(2009).
- [5] S.S. Abdel Rehim, O.A. Hazzazi, M.A. Amin and K.F. Khaled, *Corros. Sci.*, **50**, 2258(2008).
- [6] H.H. Hassan, E. Abdelghani and M.A. Amin, *Electrochim. Acta*, **52**, 6359(2007).
- [7] M.A. Amin, S.S. Abd El Rehim, E.E.F. El-Sherbini and R.S. Bayoumi, *Electrochim. Acta*, **52**, 3588(2007).
- [8] K.F. Khaled and M.A. Amin, *Corros. Sci.*, **51**, 1964(2009).
- [9] Mohammed A. Amin, K.F. Khaled and Sahar A. Fadel-Allah, *Corros. Sci.*, **52**, 140(2010)
- [10] M.A. Quraishi and R. Sardar, *Corrosion* **58**, 748(2002).
- [11] E. Norr, *Corros. Sci.* **47**, 33(2005).
- [12] M. Lebrini, M. Lagrenee, H. Vezin, L. Gengembre and F. Bentiss, *Corros. Sci.* **47**, 485(2005).
- [13] F. Bentiss, M. Bovanis, B. Mernari, M. Traisnel, H. Vezin and M. Lagrenee, *Appl. Surf. Sci.*, **253**, 3696(2007).
- [14] Z. Ait Chikh, D. Chebabe, A. Dharmraj, N. Hajjaji, A. Srhirri and M.F. Montemor, M.G.S. Ferreira, A.C. Bastos, *Corros. Sci.* **47**, 447(2005).
- [15] M. Lagrenee, B. Mernari, M. Bouanis, M. Traisnel and F. Bentiss, *Corros. Sci.* **44**, 573(2002).
- [16] M.A. Quraishi, I. Ahamad, A.K. Singh, S.K. Shukla, B. Lal and V. Singh, *Mater. Chem.Phys.* **112**, 1035(2008).
- [17] S.K. Shukla, A.K. Singh, I. Ahamad and M.A. Quraishi, *Mater. Lett.*, **63**, 819(2009).
- [18] G. Moretti, F. Guidi and G. Grion, *Corros. Sci.*, **46**, 387(2004).
- [19] E.S. Ferreira, C. Giacomelli, F.C. Giacomelli and A. Spinelli, *Mater. Chem. Phys.* **83**, 129(2004).
- [20] E.E.F. ElSherbini, *Mater. Chem. Phys.* **60**, 286(1999).
- [21] M.S. Morad, *Corros. Sci.* **50**, 436(2008).
- [22] R. A. Prabhu, A.V. Shanbhag and T.V. Venkatesha, *J. Appl. Electrochem.*, **37**, 49(2007).
- [23] S.K. Shukla and M.A. Quraishi, *Corros. Sci.*, **51**, 1007(2009).
- [24] M. M. El-Naggar, *Corros. Sci.*, **49**, 2226(2007).
- [25] M. Abdallah, *Corros. Sci.*, **46**, 1981(2004).
- [26] I.B. Obot, N.O. Obi-Egbedi and S.A. Umoren, *Corros. Sci.*, **51**, 1868(2009).

- [27] M. Abdallah, *Corros. Sci.*, 44, 717(2002).
- [28] M. Abdallah, A. S. Fouda, S.A. Shama and E. A. Afifi, *African J. Pure and Appl. Chem.*, 2, 83(2008).
- [29] E. E. Ebenso, Hailemichael Alemu, S. A. Umoren and I. B. Obot, *Int. J. Electrochem. Sci.*, 3, 1325(2008).
- [30] E. Erdem, E. Yildirim Sari, R. Kilincarslan and N. Kabay, *Transition Met. Chem.* 34, 167(2009).
- [31] A. S. Abdul Nabi and A. A. Hussain, *J. Basrah Res.(Sciences)*,38, 125(2012)
- [32] P. Lowmunkhong, D. Ungthararak and P. Sutthivaiyakit, *Corros. Sci.*, 52, 30(2010).
- [33] M. Schorr and J. Yahalom, *Corros. Sci.*, 12, 867(1972).
- [34] Lichao Hu, Shengtao Zhang, Weihua Li and Baorong Hou, *Corros. Sci.*, 52, 289 (2010).
- [35] S. S. Al-Luaibi, S. Azad and A. H. Taobi, *J. Mater. Environ. Sci.*, 2, 148(2011).
- [36] S. S. Al-Juaid, *Portugaliae Electrochimica Acta*, 25, 363(2007).

تحضير بعض اصباغ الآزو المشتقة من ادوية السلفا وتشخيصها واستخدامها كمثبطات تآكل في محلول

0,5 مولاري من حامض الهيدروكلوريك

عدنان سلطان عبدالنبي* و اخلاص قنبر جاسم**

*قسم الكيمياء ، كلية التربية ، جامعة البصرة

** فرع الكيمياء الصيدلانية ، كلية الصيدلة ، جامعة البصرة

المستخلص

تم تحضير ثلاث اصباغ آزوية مشتقة من ادوية السلفا والبيريدوكسال، شخضت المركبات المحضرة باستخدام التحليل العنصري الدقيق والاشعة تحت الحمراء وطيف الرنين النووي المغناطيسي البروتوني. استخدمت الصبغات المحضرة كمثبطات لتآكل الفولاذ الكربوني في محلول 0,5 مولاري من حامض الهيدروكلوريك، حيث تم قياس سرعة التآكل بطريقتي فقدان الوزن ومنحنيات تافل بدرجات حرارية مختلفة (30، 40، 50، 60) °م. اثبتت النتائج ان الصبغة المحضرة A2 تثبط عملية التآكل بكفاءة عالية تصل الى 80% بتركيز 10×5^{-3} مولاري وزمن 5 ساعات وحرارة 30°م. درس تأثير تغير درجة الحرارة على النسب المئوية لكفاءة تثبيط الصبغات المحضرة، حيث بينت النتائج ان النسبة المئوية لكفاءة التثبيط تقل بازياد درجة الحرارة. كما لوحظ ايضا، ان امتزاز الجزيئات على سطح المعدن يخضع لمعادلة امتزاز لانكماير. درست الدوال الترموديناميكية، طاقة التنشيط وثابت ارينياس وحرارة التفاعل والعشوائية والطاقة الحرة وثابت الاتزان لعملية الامتزاز وتم مناقشة النتائج. استخدم مبدأ الدوال الترموديناميكية لاعطاء معلومات مهمة عن طبيعة تصرف المثبطات قيد الدراسة.